

A Conditional Gating Mechanism Assures the Integrity of the Molecular Force-Sensor Titin Kinase

Stefan W. Stahl,^{†‡} Elias M. Puchner,[†] Alexander Alexandrovich,[§] Mathias Gautel,[§] and Hermann E. Gaub^{†‡*}

[†]Chair for Applied Physics and Center for NanoScience, Ludwig-Maximilians-University Munich, Munich, Germany; [‡]Center for Integrated Protein Science Munich, Munich, Germany; and [§]Cardiovascular Division and Randall Division for Cell and Molecular Biophysics, King's College London, London, United Kingdom

ABSTRACT As more and more recent investigations point out, force plays an important role in cellular regulation mechanisms. Biological responses to mechanical stress are often based on force-induced conformational changes of single molecules. The force sensor, titin kinase, is involved in a signaling complex that regulates protein turnover and transcriptional adaptation in striated muscle. The structural architecture of such a force sensor determines its response to force and must assure both activity and mechanical integrity, which are prerequisites for its function. Here, we use single-molecule force-clamp spectroscopy to show that titin kinase is organized in such a way that the regulatory domains have to unfold before secondary structure elements that determine the overall fold and catalytic function. The stepwise unfolding over many barriers with a topologically determined sequence assures that the protein can react to force by conformational changes while maintaining its structural integrity.

INTRODUCTION

Over the recent decades, much has been learned about the networks regulating cellular behavior. Although the focus of research still lies on cellular or molecular responses to biochemical stimuli, it is increasingly recognized that other inputs such as force play an important role in regulatory signaling networks. Forces affect many physiological processes such as cell proliferation and differentiation (1), cell adhesion (2), wound-healing (3), or hearing (4). Therefore, extra- and intracellular force sensors are required that generally operate through force-induced conformational changes on the molecular level (5–7). The molecular architecture of such sensors is of special interest, because it gives further insight into their working principle, and force-dependent measurements help us to understand the fundamental effects on the relation among conformation, mechanical stability, and function (8–10).

In striated muscle, the large protein titin spans half the sarcomere, provides the muscle with passive elasticity, and serves as a molecular ruler for the sarcomere assembly (11,12). Furthermore, titin is involved in mechanical signaling pathways (13). Near the C-terminus, which is located at the M-band of the sarcomere, titin contains a kinase domain that is linked to the control of muscle gene expression and protein turnover (14). The exact molecular structure and even the constituents of the M-band are not yet completely known (15,16). However, the M-band acts as an elastic crosslinker of myosin filaments, and is exposed to shear forces between adjacent myosin filaments under active contraction that lead to buckling of the M-band

on the order of at least 10 nm (15,16). Furthermore, thick filaments also undergo length changes during contraction and, to a lesser extent, stretch (17–19). The M-band and particularly M-band titin have therefore been proposed as a structure that senses muscle workload and feeds into pathways that control load-dependent remodeling (15,16).

The role of titin kinase (TK) as a force sensor was recently investigated with a combination of single-molecule force spectroscopy, molecular dynamics simulation, and enzymatic analysis (20–22). The working principle on the molecular level is shortly described as follows. In its inactive conformation, TK is autoinhibited by a dual mechanism. A C-terminal regulatory tail blocks the ATP binding site, and tyrosine-170 inhibits the catalytic base. In contrast to the situation of many other kinases, the relief of intramolecular inhibition does not occur by conformational changes induced by ligand binding, as no physiologically relevant protein activator has been identified for TK or its invertebrate analog, twitchin kinase (reviewed in Gautel (23)). Instead, forces applied between the C- and N-terminus of the protein were shown to first break a β -sheet of the C-terminal autoinhibitory tail, and then to remove the autoinhibitory α -helix R2, thus making the ATP binding pocket accessible. Single-molecule force spectroscopy measurements (24,25) performed with an atomic force microscope (AFM) (26) at physiologically relevant forces, speeds, and temperatures can therefore probe the conformational space of TK and allow predictions in the natural environment.

Previous AFM experiments at constant pulling speed revealed that the unfolding of TK occurs in a sequential and apparently predetermined manner with up to six substeps that will be called barriers in the following (Fig. 2 a). The barriers are labeled from 1 to 5 and barrier 2* is highlighted, because its occurrence was linked to the presence of ATP and the pulling speed and is sensitive to mutations in the

Submitted May 19, 2011, and accepted for publication September 6, 2011.

*Correspondence: gaub@lmu.de

Elias M. Puchner's current address is Department of Cellular and Molecular Pharmacology, University of California, San Francisco, CA.

Editor: Hideo Higuchi.

ATP-binding site, indicating that it reports conformational changes in the active site. However, the cause of the mentioned regularity in unfolding could not be directly addressed. Further and deeper insight into the structural architecture of TK would therefore result in a much better understanding of the working principle of force-driven processes on the single-molecule level.

The models of mechanical hierarchy and structural topology

Looking at the arrangement of two of the structural elements that cause energy barriers in a folded protein, there are two possible scenarios that lead to an ordered sequence of unfolding events:

In the first scenario, which we call mechanical hierarchy, the structural elements are arranged in series such that the force is transmitted through both of them and such that they may unfold independently. The reason for an ordered unfolding sequence in this case would be a different strength of the two barriers, or regarding the complete unfolding pathway of TK, a continuously rising mechanical resistance from barrier 1–5.

In the second scenario, the barriers are arranged such that the unfolding is predetermined through structural topology, meaning that the elements are shielding each other and that the first barrier has to be overcome before the second one will be under load. Schematics of these scenarios are shown in Fig. 1.

Whereas the previous studies on TK in the constant velocity mode of AFM-based force spectroscopy were ideal to determine the barrier positions with nm accuracy, they were not able to discriminate between mechanical hierarchy and structural topology because force and extension were the recorded parameters. In experiments with constant retraction velocity, the mechanical stability is characterized by force and loading rate (dF/dt) (27). That complicates the interpretation of the unfolding pattern because the latter is not constant over time. Therefore a meaningful discrimination between the two scenarios may only be obtained in the time-domain, i.e., through the access to the force-induced unfolding kinetics of the barriers.

Here we employ the so-called force-clamp mode of single-molecule force spectroscopy introduced by Fernandez and Hansma (28), where a feedback loop keeps the pulling force constant by readjusting the tip or surface position after partial unfolding of the protein (29). This mode is ideally suited for a differentiation between the given scenarios because it allows access to the time-dependent unfolding probability of the different structural elements under constant pulling force. This unfolding probability should significantly differ between the cases of mechanical hierarchy and structural topology, as will be explained in the following. Exposure to force over a longer timescale but at low extension is also likely to more accurately reflect

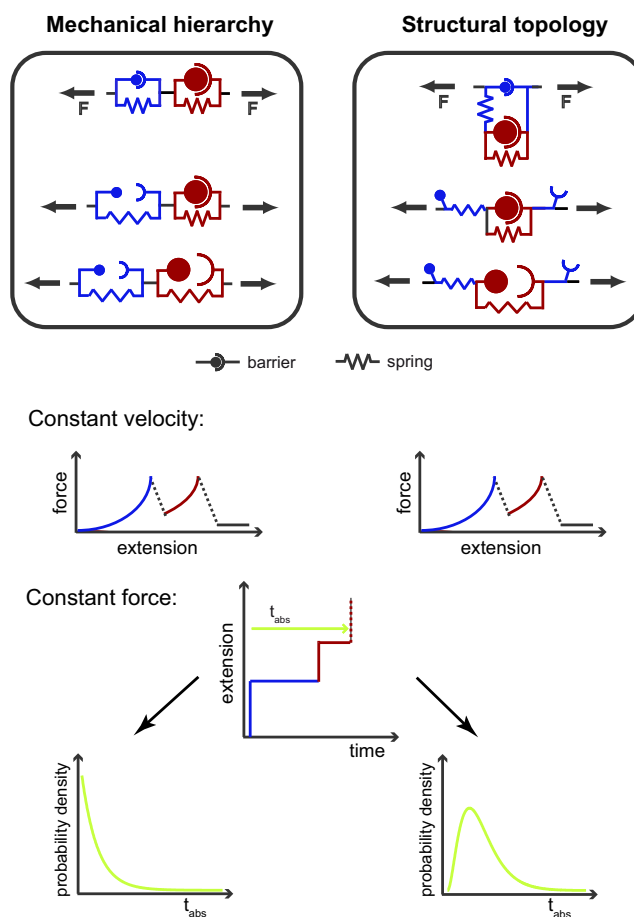


FIGURE 1 Possible mechanical architectures of proteins that consist of multiple unfolding barriers. Each structural element that causes an energy barrier in the unfolding pathway can be drawn as a combination of a bond and a nonlinear spring. In the case of mechanical hierarchy, both barriers are loaded simultaneously and the preference of opening is due to different mechanical strength. In the case of structural topology, the unfolding sequence is determined because one barrier is shielding the other. Under constant velocity single-molecule force spectroscopy conditions, the two scenarios cannot be easily distinguished because the mechanical strength is determined not only by the rupture forces but also by the loading rates of the bond that might be complex functions of the extension and speed for multibarrier proteins. Force-clamp recordings, however, can intrinsically resolve the underlying architecture because the time-dependent unfolding probabilities of the barriers are independent in the case of mechanical hierarchy and depend on each other in the case of structural topology. The distributions are expected to be single-exponential for independent two-state systems and peaked for elements that depend on the opening of another barrier.

the situation of cytoskeletal elements like titin in a contracting sarcomere.

MATERIALS AND METHODS

Single-molecule force-spectroscopy experiments

Expression and purification of the TK protein construct A168M2 (867 amino acids, from position 24422–25288 in human cardiac N2-B titin, accession No. NP 003310.3) is described in the Supporting Material of Puchner et al. (21) except that cells from the line IPLB-Sf21AE were used instead of those of

the sf9 line. Measurements were performed on mercaptosilanized glass surfaces that were functionalized with *n*-(5-(3-Maleimidopropionylamino)-1-carboxy-pentyl)iminodiacetic acid (Maleimido-C3-NTA; Dojindo, Rockville, MD) using the protocol described in Schlierf et al. (30). They specifically bind the His-Tag of the TK protein construct. After complexation of Ni²⁺ in 100 mM NiSO₄ solution and rinsing, diluted protein solution (400 μL; 50 μg/mL) was used for the measurement.

The buffer solution consists of 40 mM 2-[4-(2-hydroxyethyl)-1-piperazinyl]ethanesulfonic acid (HEPES)/KOH, 2 mM MgCl₂, 2 mM dithiothreitol, and 2 mM Adenosine-5'-triphosphate (ATP; Roche Diagnostics, Mannheim, Germany) and was adjusted to pH 7.2. Single-molecule force spectroscopy (SMFS) experiments were performed with Biolever A and B type cantilevers (Olympus, Tokyo, Japan) and a custom-built AFM (29), which can be combined with an optical microscope for single-molecule fluorescence studies (31). Spring constants of the cantilevers were determined on basis of the equipartition theorem (32) by fitting the thermal noise spectrum with the response function of a simple harmonic oscillator. A practical implementation can be found in Cook et al. (33). The obtained values are 5.2 pN/nm for the A-type and 22 pN/nm for the B-type lever.

For the force-clamp on TK, a control loop that steers a fast linear piezo (P-753; Physik Instrumente, Karlsruhe, Germany) was implemented. It adjusts the sample position in *z* direction in order to keep the pulling force constant. The fast stage is attached to another piezo stage (P-733; Physik Instrumente) that is used for sampling the surface in *xy* direction to prevent multiple picking at the same molecule and to cover a wide area. The protocol was programmed with Igor Pro 5.0 (Wavemetrics, Lake Oswego, OR) and feedbacks were operated at the MFP3D AFM controller (Asylum Research, Santa Barbara, CA). Traces were recorded at setpoints of 20, 30, 40, and 50 pN clamping force. Response times for the piezo feedback are ~5 ms. Standard deviations from the force-setpoint during force-clamp are ~3 pN for the A-type and 6 pN for the B-type lever.

Force- and extension traces were only saved if the desired force setpoint was reached and the extension at the end of the trace exceeded 30 nm to ignore traces with no tip-protein interaction and traces where unspecific tip-surface interaction prevented the lever from detaching from the surface within the acquisition time.

Force-clamp step analysis

Tip-surface extension traces were calculated by subtracting the cantilever deflection from the piezo position values. The extension traces were analyzed with an automated step finding routine written in Igor Pro 6.2 (Wavemetrics). Therefore, histograms of the position traces were generated and peaks within these histograms were detected with a modified-form of

the Peak AutoFind-Package delivered with Igor Pro. Peak position and corresponding time were saved for all traces. Unfolding time was set to zero when a position 10 nm over the surface was reached to cancel out unspecific tip-surface interaction that might keep the cantilever sticking to the surface without applying a force to the measured protein. In this way, influence of unspecific tip interaction on the absolute times of unfolding is reduced.

For the calculation of the unfolding rates k_i , only those traces were considered that had a step matching the expected increment of the unfolding of TK's barrier no. 5 (i.e., 44 ± 3 nm at 30 pN pulling force) and an overall extension of at least 70 nm. For identification of the other barriers, the position before the opening of barrier no. 5 was set to zero (compare to Fig. 4). Steps were classified by selecting height and position relative to barrier 5 according to Table 1.

Rate fitting

The probability density distribution of the unfolding time for each barrier was determined as follows. Histograms over the time between two consecutive events (barriers 2–5) and the absolute time of unfolding (barrier 1) were calculated. They neglect events that are shorter than the experimentally determined average response time of the feedback (compare to Fig. S2 in the Supporting Material), because these events occur only very seldom and would distort the probability distribution. The number of bins in each histogram corresponds to the square root of the number of events. The unfolding rates k_i were determined by fitting a single-exponential function with time offset t_0 to the histogram:

$$p_{i,rel}(t) = k_i e^{-k_i(t-t_0)}.$$

The time offset t_0 again respects the finite response time of the feedback and is linear-dependent on the height of the step (see Fig. S2). Errors of the probability density histograms and the off-rates were determined by bootstrapping. Therefore, for each histogram, 100 random subpopulations were generated that consist of only 30% of the original data points. The same rate fitting was applied to the subpopulations. Error bars include the inner 90% of the bootstrapped values.

Markov-chain model

To check for consistency with the thesis that the structural elements of titin kinase (TK) are topologically ordered, the following model was developed. It describes the unfolding of TK from the natural folded conformation (F) to the completely stretched unfolded conformation (U) as a sequential Markov chain with up to five substeps (compare to Scheme 1 below) that are

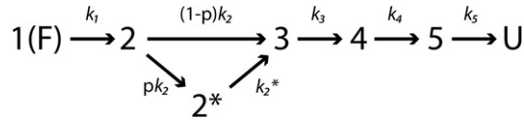
TABLE 1 Identification data for the substeps of TK unfolding at 30 pN clamping force

Barrier No.	1	2→3	2→2*	2*
Contour length increment (21)	9.1 nm	28.6 nm	19.4 nm	10.1 nm
Expected increment at 30 pN*	6.8 nm	21.5 nm	14.6 nm	7.6 nm
Identification interval in force-clamp experiment	8 ± 2 nm (A ₂)	22 ± 2.5 nm (C)	14 ± 3 nm (B)	8 ± 2 nm (A ₂)
Identification position relative to barrier 5	-42 ± 4 nm	-20 ± 4 nm	-27 ± 5 nm	-19 ± 3 nm
Determined off-rate at 30 pN k_{off}	31 ± 8 s ⁻¹	20 ± 4 s ⁻¹	18 ± 6 s ⁻¹	83 ± 45 s ⁻¹
Barrier No.	3	4	5	Fn
Contour length increment (21)	7.3 nm (7.5 nm)	18.0 nm (16.4 nm)	57.9 nm (58.3 nm)	30.8 nm
Expected increment at 30 pN*	5.5 nm (5.6 nm)	13.5 nm (12.3 nm)	43.4 nm (43.7 nm)	23.1 nm
Identification interval in force-clamp experiment	4 ± 2 nm (A ₁)	14 ± 3 nm (B)	44 ± 3 nm (D)	22 ± 2.5 nm (C)
Identification position relative to barrier 5	-15 ± 3 nm	0 ± 2 nm	44 ± 3 nm	67 ± 7 nm
Determined off-rate at 30 pN k_{off}	21 ± 4 s ⁻¹	20 ± 4 s ⁻¹	14 ± 2 s ⁻¹	1.2 ± 0.4 s ⁻¹

Barriers were identified according to Fig. 4 and rates were obtained by fitting single-exponential decays to the probability distribution histograms of relative barrier opening times (see Materials and Methods). Values in parentheses correspond to the unfolding pathway with the additional barrier 2* or denote the population identifier.

*According to a wormlike-chain fit with persistence-length $p = 0.6$ nm.

identical with the measured barriers of previous work on TK (21) and describe distinct conformational states of TK. The part of the amino-acid chain that already went into an unfolded state can be described by polymer models as the wormlike-chain model and increases with every step until the complete protein is stretched. The decay of each step under force-clamp conditions is assumed to be single-exponential with a rate constant k_i . After the decay of state 2, the additional substep 2^* is reached with probability p that is dependent on the pulling velocity (21).



Thus, the system can be described by the following linear differential equation system,

$$\frac{d}{dt} \begin{pmatrix} p_1 \\ p_2 \\ p_{2^*} \\ p_3 \\ p_4 \\ p_5 \end{pmatrix} = \begin{pmatrix} -k_1 & & & & & \\ k_1 & -k_2 & & & & \\ & pk_2 & -k_{2^*} & & & \\ & (1-p)k_2 & k_{2^*} & -k_3 & & \\ & & & k_3 & -k_4 & \\ & & & & k_4 & -k_5 \end{pmatrix} \begin{pmatrix} p_1 \\ p_2 \\ p_{2^*} \\ p_3 \\ p_4 \\ p_5 \end{pmatrix},$$

where $p_i(t)$ describes the time-dependent probability distribution of being in state i . The differential equation system was solved under the initial condition $p_i(0) = 1, p_j(0) = 0 (i \neq 0)$ analytically with the computer algebra

system MAPLE 14 (Maplesoft, Waterloo, Canada). The normalized solution of $p_5(t)$ for the experimentally determined rate constants k_i is depicted in Fig. 5. Because the probability density for going from state 5 to the unfolded conformation at time t is proportional to the probability of being in state 5 at time t , $p_5(t)$ can be directly compared with the experimentally determined unfolding times.

RESULTS

Distinction of structural barriers by step height

In one cycle of a force-clamp experiment, the tip of an AFM cantilever is brought into contact with the surface and retracted by a feedback loop that keeps the force constant. Typical unfolding traces of the tip-surface distance and the force are shown in (Fig. 2 c). The force is clamped over time and only shortly drops when a barrier opens, due to the finite response time of the feedback loop. For investigating the properties of the mechanically stable building blocks of TK, it is essential to discriminate the barrier-causing elements in the recorded data. Therefore, we analyzed the unfolding traces with an automated step-finding tool that detects plateaus in the extension versus time traces and records relevant parameters like step position and height or the time at which the unfolding occurred (see Materials and Methods).

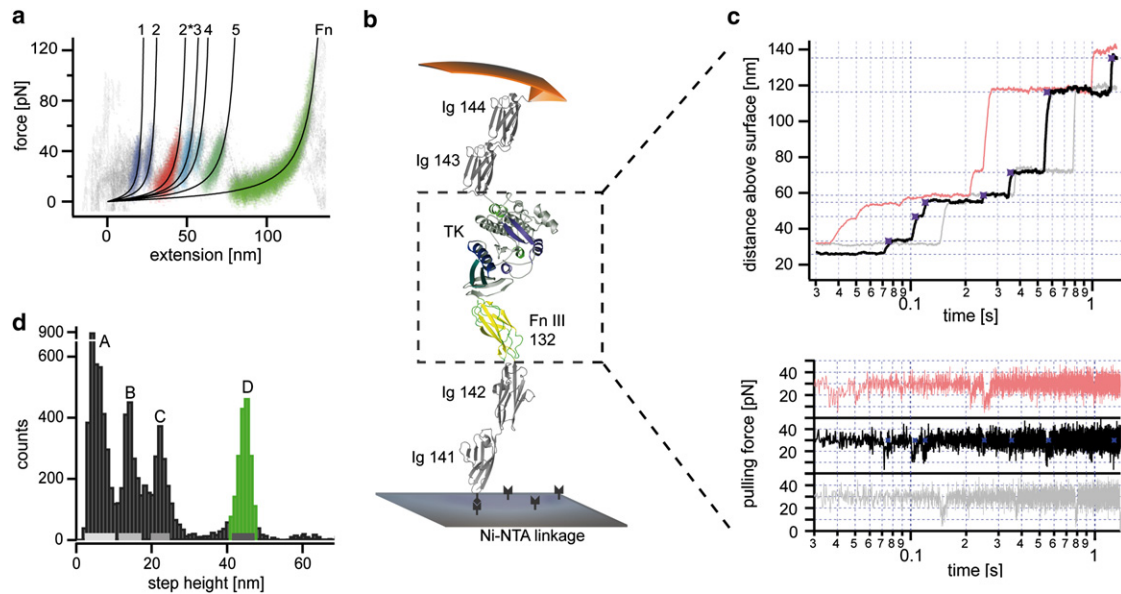


FIGURE 2 Sample data for the force-clamp experiments performed on titin kinase. (a) An overlay of 44 unfolding traces obtained by single-molecule force spectroscopy (SMFS) in constant retraction velocity mode points out that there is a preferred sequence of unfolding. The barriers that have to be overcome are numbered according to their position in this sequence. The probability of occurrence of barrier 2^* is linked to ATP presence in solution and pulling velocity and therefore treated specially (21). Data points are displayed semitransparent. Such areas with high point density appear more intense. (b) For the SMFS experiments the titin construct A168-M2, which consists of the kinase domain (PDB No. 1TKI), four Ig-like domains and one fibronectin-type III domain, is immobilized on the surface by specific coupling of the His-tag to a NTA-functionalized surface and is pulled with a cantilever under constant force conditions. (c) Sample traces of the stepwise kinase unfolding under force-clamp conditions at a setpoint of 30 pN. Due to the difference in stability, unfolding of the Ig-domains is only very rarely observed at this force. The distance of the two thin traces is set off to match the position of the black trace. (d) Histogram of the heights of all steps detected in the $\sim 10,000$ unfolding traces that were recorded at 30 pN clamping force. Four populations are clearly observable (A–D). A comparison with the unfolding pattern obtained in constant velocity mode confirms consistency and shows that the peaks below 30 nm are formed by more than one structural element whereas the peak D is only due to the long increment of barrier 5 in titin kinase (compare to Table 1). Therefore, this peak is used for trace selection and first structural dependency analysis.

A histogram of the detected step heights at a pulling-force of 30 pN is given in Fig. 2 *d*. It is apparent that the heights are not evenly distributed but exhibit several populations, four of which are clearly distinguishable (*A–D*). A comparison with the unfolding pattern obtained by regular force-spectroscopy with constant pulling velocity allows the identification of some of the barriers by their step height. For the identification, we keep the notation of the barriers as they were introduced in Puchner et al. (21). The structural element of TK with the largest contour length (barrier 5 in Fig. 2 *a*) matches the position of population *D* around 44.5 nm (Table 1). We will initially focus on this barrier because it is of special interest: it always opened last in velocity-clamp experiments and it may be unambiguously identified by its step height only. The other populations may be due to the unfolding of at least two different structural elements of the titin construct and will be examined later.

Barrier 5 is mechanically shielded by other structural elements

In AFM experiments with constant velocity, barrier 5 of titin kinase was always observed to unfold last, but it cannot be easily distinguished whether this is due to higher mechanical stability or due to the fact that the domain is topologically shielded by other structural elements. The force-clamp recordings, however, are intrinsically able to distinguish between these two scenarios through the access to the unfolding kinetics, i.e., the probability of unfolding versus time. In the case of mechanical hierarchy, the likelihood of unfolding should not depend on other structural elements and thus yield a single exponential decay, whereas the dependence of unfolding on other structural elements in the case of structural topology would result in a peaked distribution because it takes a certain time until the observed state gets populated.

Fig. 3 *a* shows the distribution of how long it takes for barrier 5 to open after force is first applied to the protein. This absolute time distribution exhibits a well-pronounced peak with a maximum unfolding probability at ~200 ms, which is far longer than the minimal time resolution of the instrument. Note that the response time for the piezo feedback is ~5 ms (compare to the Supporting Material for experimental details). There is no doubt that the measured time distribution is not single-exponential, as would be required for independent Markovian two-state barriers (35) in a mechanical hierarchy. Deviations from two-state processes such as static (36) or dynamic (37) disorder and glassy dynamics (38) are not appropriate explanations for the measured data, because they still have monotonic decaying probability distributions. The asymmetrical shape with its pronounced peak (Fig. 3 *a*) resembles a γ -distribution very well. A simple model that yields such a distribution is that of several single-exponential decaying processes that occur one after another. For example, the

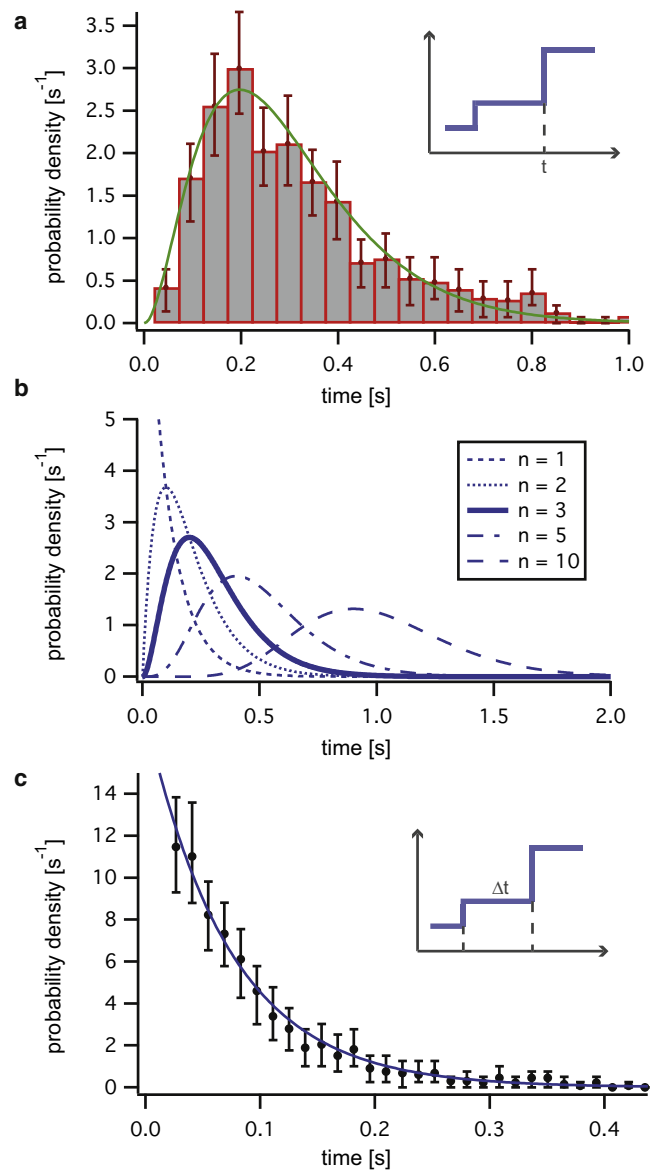


FIGURE 3 Structural dependencies of barrier no. 5 measured at a constant force of 30 pN. The timescales of the unfolding of the 44 nm increment (see Fig. 2 *d*, population *D*) were analyzed as follows. (a) Histogram of unfolding times after first force-appliance (t_{abs}). The distribution is clearly not single-exponential but γ -shaped, which is a premise for structural topologies. The fitted line describes a three-step Erlang-distribution with rate $k = 10.1 \text{ s}^{-1}$. (b) Erlang-distributions for different step numbers n from 1 to 10. For $n = 1$ the distribution reduces to a single-exponential decay. With increasing n average, unfolding times get higher and the distribution gets more symmetric until it resembles a shifted normal distribution. (c) Probability density histogram for the times t_{rel} between the unfolding of the preceding step and the unfolding of barrier 5. The decay probability is single-exponential and indicates that the single substeps are unfolding according to the principle of Markovian two-step behavior.

time-dependent probability density for the n^{th} subsequent occurrence of a process with the rate k is given by a binomial distribution for discrete time steps (39) or, in continuous time, by an Erlang-Distribution (37,40)

$$p(t; k, n) = \frac{k^n}{(n-1)!} t^{n-1} e^{-kt},$$

which is a special case of a γ -distribution with a discrete second parameter. The behavior is depicted in Fig. 3 *b*. For $n = 1$ the probability density reduces to a simple exponential curve. For $n > 1$, the curve has a peak and its position shifts to higher times with higher numbers of events. Furthermore, the curve gets less asymmetric with higher n . Fig. 3 *c* shows the distribution of the dwell time between the opening of barrier 5 and the previous barrier. It is again supporting a model with structural dependent barriers because it exhibits an exponential decay with a rate constant of $k_5 = 14 \pm 2 \text{ s}^{-1}$, and thus indicates that the single unfolding steps obey Markovian rules.

The absolute time distribution of the unfolding of barrier 5 is represented very well by an Erlang distribution (3 steps; $k = 10.1 \text{ s}^{-1}$) and its time constant does roughly match the measured unfolding rate of barrier 5. However, the Erlang-Model is an oversimplification by assuming all rates to be the same, and is thus not an accurate fitting model for the unfolding of TK. Nevertheless, it already illustrates that there has to be a structural dependency of the unfolding steps.

Identification of the other structural elements and Markov chain modeling

To gain further insight into the processes taking place during unfolding, the other barriers in the force-clamp traces have to be identified too. This is done by taking into account both the step height and the position at which unfolding occurs. Barrier 5 is overcome at a position 114 nm above the surface with a distribution width of 10 nm that is due to different attachment sites of cantilever and surface and partial opening of the surrounding Ig/Fn-domains (see Fig. S5). This defined position exactly matches the added unfolding lengths of all structural elements of TK at 30 pN pulling force (see Table 1) and further affirms that barrier 5 also opens last in force-clamp experiments. Fig. 4 *a* displays how the barriers 1–4 as well as the fibronectin or Ig domains can be identified by offsetting the distance trace to the position of the unfolding event before barrier 5.

For nearly all of the events, this relative position together with the step height allows the interpretation of which unfolding step belongs to which barrier. (A drawback of this method is that one only selects those traces that have the unfolding order from 1 to 5, but the histograms in Fig. 4 *a* prove that at least 88% of all detected steps in the selected traces agree with this scheme.) To reduce possible misinterpretation of the barrier number, the step height population A was split into two parts (A_1, A_2) with a cutoff at 6 nm. Therefore, there are maximally two expected barriers per histogram, and their expected positions are

well separated. The histograms exhibit very pronounced peaks that match the sequential unfolding pattern, which is observed in experiments with constant retraction velocity. Now the unfolding rates of the remaining barriers can be determined (Fig. 4 *b*). They are depicted in Table 1 together with the values and population identifiers that were used to determine the barrier number.

To check the model of structural topology, we calculated the analytical solution of the coupled differential equations of a sequential Markov chain consisting of six barriers with exponentially distributed unfolding times (see Materials and Methods). There are six steps, because the additional energy barrier 2* that is observed with a velocity-dependent probability is considered as well. The resulting probability distribution of the unfolding time of the last step with the experimentally determined opening rates is depicted in Fig. 5. Maximum and minimum likelihood distributions were calculated by different combinations of rates that were chosen from the experimental error range such that they lead to most or least probable unfolding for a given time. As the graph shows, the degree of coincidence of the sequential Markov chain model with the experimentally determined distribution is high. The most probable unfolding time, for example, is 204 ms for the model and within 170–220 ms for the experimental data. However, the experimental distribution has a slightly broader tail that is shifted to longer times.

A manual revision of the unfolding traces showed that the timescale of unfolding seems to correlate for the structural elements in a single trace. All these elements tend to either open slightly faster or slower in a single trace, which causes a broadening of the probability distribution to longer times with respect to the Markov chain model. Because it cannot be distinguished whether this shift is due to an intramolecular effect like deviations from two-state behavior (38,39) or is mainly caused by faint shifts of the force setpoint due to cantilever drift, we will refrain from a further discussion of this effect and treat it as incompleteness of the model or experimental artifact. (Note that setpoints that are shifted only ~5 pN can already yield rates that differ ~50% from the desired one. Therefore, protein unfolding in traces where the setpoint is 5 pN too low would need, on average, twice the time and 0.66 of the regular time for setpoints that are too high. This effect is strong enough to explain the deviations from the modeled line. See Force Dependence of Unfolding Rates in the Supporting Material.)

Independent unfolding of the fibronectin domain

At 30 pN clamping force, in ~10% of the unfolding traces, not only is the complete titin kinase unfolding pattern observable, but another 22-nm step is present. This is due to the unfolding of one of the four surrounding Ig-domains or the fibronectin domain, which are included in the titin fragment used here and have similar step heights as barrier

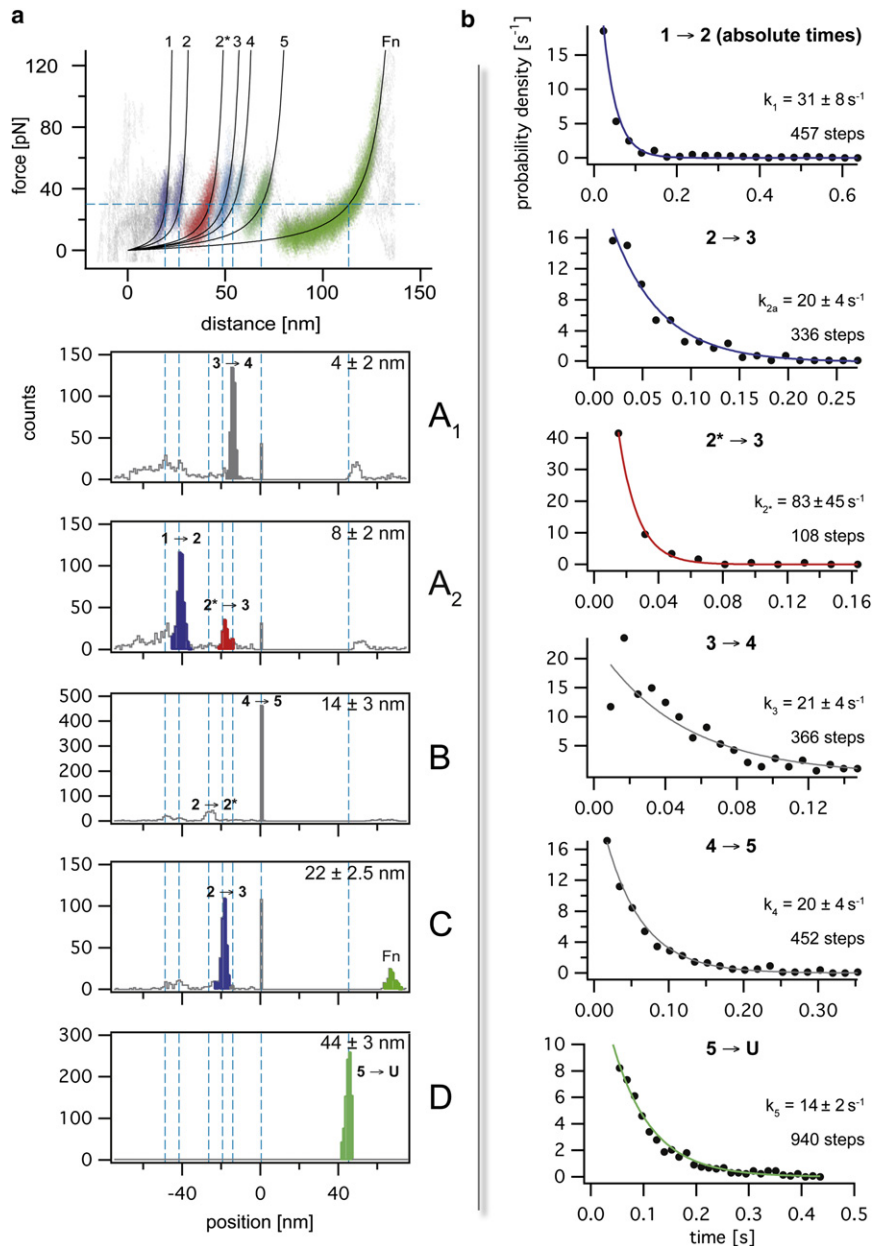


FIGURE 4 (a) Identification of the structural barriers by height and position relative to barrier 5. Histograms of the unfolding position relative to barrier 5 are drawn for each population introduced in Fig. 2 d. To reduce the possibility of misinterpretation between barriers 2* and 3, the population A has been split into two parts with a cutoff at 6 nm. The population identifier (A–D) is marked on the right of each histogram, and the contained step height is given (top right). The histograms exhibit well-defined peaks at the positions where they are expected for the scenario of structural topology with the constant velocity unfolding pattern as a ruler. The measurement was performed with 2 mM ATP present in solution. The probability of occurrence of peak 2* is linked to pulling velocity and ATP content (21) and was determined to be $p = 0.35$, which matches the expectations from constant velocity experiments very well. (b) Probability density histograms with single-exponential decay fits for the substeps of TK unfolding from the folded conformation (F) to the completely unfolded conformation (U) at 30 pN pulling force. Details of histogram generation and fitting are given in Rate Fitting (see main text).

2 (compare to Table 1). Those steps most likely describe the unfolding of the fibronectin domain, because its fold is inherently less stable than the Ig-fold (43,44). Although in the majority of the traces the additional unfolding occurs after the titin kinase barriers, a revision of the traces with two steps in the identification interval at ~22 nm pointed out that the position of this increment is random. In ~8% of the traces, the additional step is located within the unfolding of the kinase domain and does not shift the sequence of barriers 1–5. Fig. 5 b shows the probability distribution for the absolute unfolding times of the additional domain.

Because the Ig and Fn domains are comparatively stable (45), unfolding occurs at longer timescales. In contrast to

the TK barriers, the additional domain is decaying exponentially, which demonstrates well that the unfolding of these domains is independent of the kinase unfolding according to the principle of mechanical hierarchy. The measured rate, however, does not correspond to the natural unfolding rate at this force. The natural rate is expected to be much lower; longer times are underrepresented in the histogram, because the detachment of protein from the cantilever or the surface occurs at a similar timescale (see Fig. S4 for comparison). Furthermore, the effect that the fibronectin fold may open in between the kinase domains means that some of the steps that are contained in the histograms of Fig. 4 a cannot be explained with the direct sequence from barrier 1 to 5.

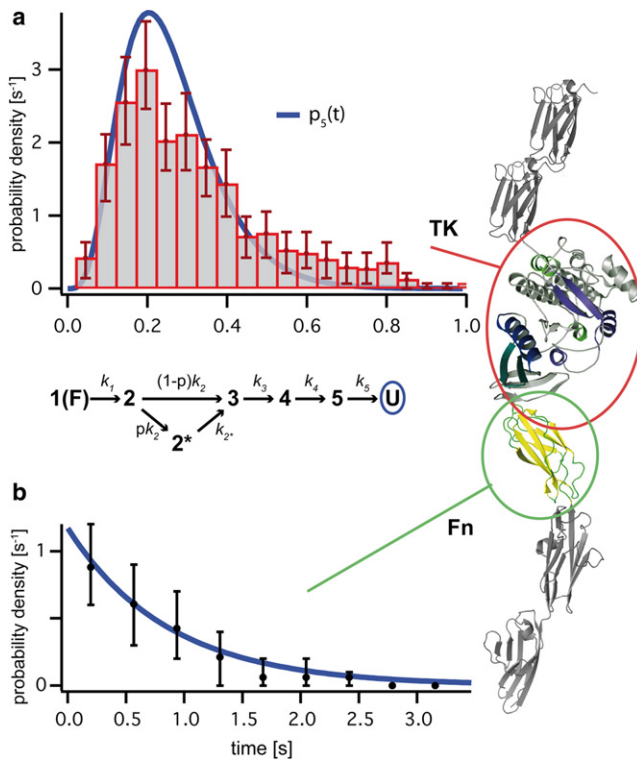


FIGURE 5 Markov-chain model and independent unfolding of the fibronectin domain. (a) The unfolding probability distribution from barrier 5 into the completely unfolded state (U) can be reasonably well fitted with the model $p_5(t)$, which consists of a sequential Markov-chain with six dependent single-exponential processes. The rates k_i are taken from Table 1. This model describes a structural topology of all barrier-causing structural elements of titin kinase. The shift to longer times in the experimental data is most likely due to slight offsets in the pulling force due to cantilever drift, which cannot be neglected at the small clamping force of only 30 pN. (b) Unfolding probability distribution for the fibronectin domains obtained at 30 pN pulling force. In contrast to the other barriers, the absolute unfolding times of the fibronectin domain are exponential-distributed, which demonstrates that this barrier unfolds independently from the structural elements of titin kinase.

DISCUSSION

In summary, our experiments and modeling have unraveled the mechanical architecture of titin kinase as an example of a biological mechanical force sensor. Our results confirm that forces below 30 pN, reflecting a force imbalance in the muscle sarcomere equivalent to only ~ 5 myosin motor domains with 6 pN each (47), can result in significant regional, but nondestructive conformational changes in TK. In fact, on a timescale of seconds, forces much lower than 30 pN are predicted to lead to opening of the TK active site, because the rate of unfolding of the TK elements strongly depends on the pulling force (see the [Supporting Material](#)). This implies that even at lower forces than those that were experimentally observable in our setup, barriers may open at longer timescales. Modeled force-responses of whole sarcomeres further suggest that the experimental forces lie in the physiological accessible range (48).

The line of evidence from our measured single-molecule force spectroscopy data proves that the underlying principle that assures enzymatic function under the constraint of applied force is the structural topology of at least some of the force-bearing elements. The measured data strongly suggest that the unfolding of the complete titin kinase construct under force occurs in a series of six exponentially distributed barriers that have to be overcome one after the other. A protein architecture like this ensures the proper function of this special enzyme, which can react to mechanical stimuli with conformational changes while maintaining its structural integrity. Before structural elements unfold that support proper conformation of the active site, barriers have to be overcome that determine the enzymatic response (21,22).

The same stabilization principle has recently been shown to be applicable also to artificially designed proteins, and may be useful for novel multifunctional designed elements in nanomechanics and nanobiotechnology (49).

Furthermore, the reliability of the experimental technique was underlined by demonstrating that the recorded data are able to prove the independent unfolding of the adjacent fibronectin fold next to the protein kinase according to the principle of mechanical hierarchy. The way in which mechanical forces control the conformational landscape of titin around its single catalytic domain suggest also that protein interactions close to the kinase domain might be subject to mechanical modulation. Integration of this molecular information into future models of the sarcomeric M-band should ultimately help us to understand how forces in this enigmatic cellular structure are both resisted and employed for signaling.

SUPPORTING MATERIAL

Additional information accompanied by five figures is available at [http://www.biophysj.org/biophysj/supplemental/S0006-3495\(11\)01105-2](http://www.biophysj.org/biophysj/supplemental/S0006-3495(11)01105-2).

S.W.S. thanks Mathias Strackham for helpful discussions.

M.G. and A.A. gratefully acknowledge the generous support by the British Heart Foundation and the Medical Research Council. M.G. holds the British Heart Foundation Chair of Molecular Cardiology. E.M.P. is supported by the Deutsche Forschungsgemeinschaft. This work was supported by the Nanosystems Initiative Munich, the Volkswagenstiftung, and the Deutsche Forschungsgemeinschaft Grant SFB 863.

REFERENCES

1. Wozniak, M. A., and C. S. Chen. 2009. Mechanotransduction in development: a growing role for contractility. *Nat. Rev. Mol. Cell Biol.* 10:34–43.
2. Smith, A. S., and E. Sackmann. 2009. Progress in mimetic studies of cell adhesion and the mechanosensing. *ChemPhysChem.* 10:66–78.
3. Yagmur, C., S. Akaishi, ..., E. Guneren. 2010. Mechanical receptor-related mechanisms in scar management: a review and hypothesis. *Plast. Reconstr. Surg.* 126:426–434.

4. Gillespie, P. G., and U. Müller. 2009. Mechanotransduction by hair cells: models, molecules, and mechanisms. *Cell*. 139:33–44.
5. Vogel, V. 2006. Mechanotransduction involving multimodular proteins: converting force into biochemical signals. *Annu. Rev. Biophys. Biomol. Struct.* 35:459–488.
6. Brown, A. E., and D. E. Discher. 2009. Conformational changes and signaling in cell and matrix physics. *Curr. Biol.* 19:R781–R789.
7. Zhang, X., K. Halvorsen, ..., T. A. Springer. 2009. Mechanoenzymatic cleavage of the ultralarge vascular protein von Willebrand factor. *Science*. 324:1330–1334.
8. Crampton, N., and D. J. Brockwell. 2010. Unraveling the design principles for single protein mechanical strength. *Curr. Opin. Struct. Biol.* 20:508–517.
9. Puchner, E. M., and H. E. Gaub. 2009. Force and function: probing proteins with AFM-based force spectroscopy. *Curr. Opin. Struct. Biol.* 19:605–614.
10. Thomas, W. E., V. Vogel, and E. Sokurenko. 2008. Biophysics of catch bonds. *Annu. Rev. Biophys.* 37:399–416.
11. Lange, S., E. Ehler, and M. Gautel. 2006. From A to Z and back? Multi-compartment proteins in the sarcomere. *Trends Cell Biol.* 16:11–18.
12. Tskhovrebova, L., and J. Trinick. 2010. Roles of titin in the structure and elasticity of the sarcomere. *J. Biomed. Biotechnol.* 2010:612482.
13. Krüger, M., and W. A. Linke. 2009. Titin-based mechanical signaling in normal and failing myocardium. *J. Mol. Cell. Cardiol.* 46:490–498.
14. Lange, S., F. Xiang, ..., M. Gautel. 2005. The kinase domain of titin controls muscle gene expression and protein turnover. *Science*. 308:1599–1603.
15. Agarkova, I., and J. C. Perriard. 2005. The M-band: an elastic web that crosslinks thick filaments in the center of the sarcomere. *Trends Cell Biol.* 15:477–485.
16. Gautel, M. 2011. The sarcomeric cytoskeleton: who picks up the strain? *Curr. Opin. Cell Biol.* 23:39–46.
17. Huxley, H. E., A. Stewart, ..., T. Irving. 1994. X-ray diffraction measurements of the extensibility of actin and myosin filaments in contracting muscle. *Biophys. J.* 67:2411–2421.
18. Brunello, E., P. Bianco, ..., V. Lombardi. 2006. Structural changes in the myosin filament and cross-bridges during active force development in single intact frog muscle fibers: stiffness and x-ray diffraction measurements. *J. Physiol.* 577:971–984.
19. Lombardi, V., G. Piazzesi, ..., M. Irving. 2004. X-ray diffraction studies of the contractile mechanism in single muscle fibers. *Philos. Trans. R. Soc. Lond. B Biol. Sci.* 359:1883–1893.
20. Gräter, F., J. Shen, ..., H. Grubmüller. 2005. Mechanically induced titin kinase activation studied by force-probe molecular dynamics simulations. *Biophys. J.* 88:790–804.
21. Puchner, E. M., A. Alexandrovich, ..., M. Gautel. 2008. Mechanoenzymatics of titin kinase. *Proc. Natl. Acad. Sci. USA*. 105:13385–13390.
22. Puchner, E. M., and H. E. Gaub. 2010. Exploring the conformation-regulated function of titin kinase by mechanical pump and probe experiments with single molecules. *Angew. Chem. Int. Ed. Engl.* 49:1147–1150.
23. Gautel, M. 2011. Cytoskeletal protein kinases: titin and its relations in mechanosensing. *Pflugers Arch.* 462:119–134.
24. Oberhauser, A. F., and M. Carrión-Vázquez. 2008. Mechanical biochemistry of proteins one molecule at a time. *J. Biol. Chem.* 283:6617–6621.
25. Neuman, K. C., and A. Nagy. 2008. Single-molecule force spectroscopy: optical tweezers, magnetic tweezers and atomic force microscopy. *Nat. Methods*. 5:491–505.
26. Binnig, G., C. F. Quate, and C. Gerber. 1986. Atomic force microscope. *Phys. Rev. Lett.* 56:930–933.
27. Evans, E., and K. Ritchie. 1999. Strength of a weak bond connecting flexible polymer chains. *Biophys. J.* 76:2439–2447.
28. Oberhauser, A. F., P. K. Hansma, ..., J. M. Fernandez. 2001. Stepwise unfolding of titin under force-clamp atomic force microscopy. *Proc. Natl. Acad. Sci. USA*. 98:468–472.
29. Stahl, S. W., E. M. Puchner, and H. E. Gaub. 2009. Photothermal cantilever actuation for fast single-molecule force spectroscopy. *Rev. Sci. Instrum.* 80:073702.
30. Schlierf, M., F. Berkemeier, and M. Rief. 2007. Direct observation of active protein folding using lock-in force spectroscopy. *Biophys. J.* 93:3989–3998.
31. Gumpp, H., S. W. Stahl, ..., H. E. Gaub. 2009. Ultrastable combined atomic force and total internal reflection fluorescence microscope [corrected]. *Rev. Sci. Instrum.* 80:063704 (corrected).
32. Butt, H. J., and M. Jaschke. 1995. Calculation of thermal noise in atomic-force microscopy. *Nanotechnology*. 6:1–7.
33. Cook, S., T. E. Schaffer, ..., K. M. Lang. 2006. Practical implementation of dynamic methods for measuring atomic force microscope cantilever spring constants. *Nanotechnology*. 17:2135–2145.
34. Reference deleted in proof.
35. Cao, Y., R. Kuske, and H. B. Li. 2008. Direct observation of Markovian behavior of the mechanical unfolding of individual proteins. *Biophys. J.* 95:782–788.
36. Kuo, T. L., S. Garcia-Manyes, ..., J. M. Fernández. 2010. Probing static disorder in Arrhenius kinetics by single-molecule force spectroscopy. *Proc. Natl. Acad. Sci. USA*. 107:11336–11340.
37. Floyd, D. L., S. C. Harrison, and A. M. van Oijen. 2010. Analysis of kinetic intermediates in single-particle dwell-time distributions. *Biophys. J.* 99:360–366.
38. Brujic, J., R. I. Hermans, ..., J. M. Fernandez. 2006. Single-molecule force spectroscopy reveals signatures of glassy dynamics in the energy landscape of ubiquitin. *Nat. Phys.* 2:282–286.
39. Brujic, J., R. I. Z. Hermans, ..., J. M. Fernandez. 2007. Dwell-time distribution analysis of polyprotein unfolding using force-clamp spectroscopy. *Biophys. J.* 92:2896–2903.
40. Evans, M., N. Hastings, and B. Peacock. 2000. *Statistical Distributions*. Wiley, New York 71–73.
41. Reference deleted in proof.
42. Reference deleted in proof.
43. Rief, M., M. Gautel, ..., H. E. Gaub. 1998. The mechanical stability of immunoglobulin and fibronectin III domains in the muscle protein titin measured by atomic force microscopy. *Biophys. J.* 75:3008–3014.
44. Linke, W. A., and A. Grützner. 2008. Pulling single molecules of titin by AFM—recent advances and physiological implications. *Pflugers Arch.* 456:101–115.
45. Garcia-Manyes, S., J. Brujić, ..., J. M. Fernández. 2007. Force-clamp spectroscopy of single-protein monomers reveals the individual unfolding and folding pathways of I27 and ubiquitin. *Biophys. J.* 93:2436–2446.
46. Reference deleted in proof.
47. Piazzesi, G., M. Reconditi, ..., V. Lombardi. 2007. Skeletal muscle performance determined by modulation of number of myosin motors rather than motor force or stroke size. *Cell*. 131:784–795.
48. Shabarchin, A. A., and A. K. Tsaturyan. 2010. Proposed role of the M-band in sarcomere mechanics and mechano-sensing: a model study. *Biomech. Model. Mechanobiol.* 9:163–175.
49. Peng, Q., and H. Li. 2009. Domain insertion effectively regulates the mechanical unfolding hierarchy of elastomeric proteins: toward engineering multifunctional elastomeric proteins. *J. Am. Chem. Soc.* 131:14050–14056.
50. Reference deleted in proof.